JASA ARTICLE

Radiation modes and sound radiation from a flexible structure mounted in a duct

Yang Liu,[1,a)] Jingtao Du,[1,b)] and Li Cheng[2]
[1]College of Power and Energy Engineering, Harbin Engineering University, Harbin 150001, China
[2]Department of Mechanical Engineering, The Hong Kong Polytechnic University, Hong Kong 999077, China

ABSTRACT:
The concept of the radiation modes, originally proposed for free-field problems, has found its widespread use in sound radiation analyses of vibrating structures and their active control applications. In this paper, the sound radiation of a flexible structure, flush-mounted inside a duct in both 2D and 3D configurations, is investigated via an energy-based formulation in conjunction with the near-field integration technique. The structural radiation characteristics are first discussed in terms of modal radiation efficiency, which exhibits obvious oscillating behavior with respect to frequencies, in which symmetric patterns are dominant with smooth variations for small acoustic wavenumbers. Then the interior sound radiation modes are investigated. It is shown that, as compared with their free-space counterparts, the lower-order radiation modes in a duct are more sensitive and prone to be affected by the duct starting from its cut-on frequency. Drastic changes in the radiation mode shapes are observed around the cut-on frequency and each of its multiples/harmonics. Finally, analyses are extended to a coupled panel-duct system. It is observed that, contrary to the free-space case, lower-order radiation modes exhibit predominant variations along the duct length direction, suggesting a possible simplification of the 3D configuration into a 2D one.
 https://doi.org/10.1121/10.0001258
(Received 9 January 2020; revised 26 April 2020; accepted 28 April 2020; published online 13 May 2020)
[Editor: Laurent Maxit] Pages: 3465–3475

I. INTRODUCTION

Sound radiation from vibrating structures into an acoustic medium is the key issue in structural acoustics and is relevant to a wide variety of engineering problems. After early attempts to solve the acoustic radiation output via independently radiating surface velocity distributions,[1–3] the concept of "radiation modes"[4,5] was proposed, which triggered extensive investigations into sound radiation from vibrating flexible structures into a free space, as well as the exploration of its use in various applications such as active control.[6] Radiation modes can be derived through the eigen-functions or singular value decomposition of the radiation resistance matrix, and their radiation efficiencies are proportional to the corresponding eigenvalues of the radiation resistance matrix.[7] Such modal construction represents particular velocity distribution patterns on the radiator surface, which radiate sound independently and are decoupled from each other. The spatial shape and the radiation efficiencies of such radiation modes only depend on the geometry, size, and shape of the radiator, but not its material properties or boundary conditions. Owing to these appealing features, only a few low-order radiation modes need to be considered to achieve an effective estimation or the control of the sound radiation of a structure.[4] Since its establishment, the concept has been widely used, mainly for sound radiation problems in free fields. For example, Currey and Cunefare[8] examined the bounding and convergence behavior of radiation efficiencies of the exterior acoustic modes of a finite baffled beam and found that the acoustic radiation modes of an arbitrary 3D structure exhibit the same frequency grouping as those for spheres.[9] Bai further employed the radiation modes for estimating the sound power and the far-field pressure radiated by a complex source, without requiring any special measuring environment.[10] Mapped radiation modes were also used by Wu *et al.*[11,12] to achieve efficient and accurate prediction of the sound radiation power. Marburg *et al.*[13] exploited the radiation modes to identify the surface area of a vibrating structure that contributes to the total radiated sound power. Meanwhile, the concept of the radiation modes has also been used in various active noise control applications. The aim of existing studies varies from achieving efficient weighting schemes for sensors to reducing the controller dimensionality to getting reduced order modeling/design of radiation filters.[14–16]

From the aforementioned works, the benefit of using radiation modes has been thoroughly demonstrated for various problems of sound radiation in a free space. In contrast, a less investigated problem is the one involving sound radiation/transmission from flexible structures into a confined space—a situation frequently encountered in practice[17–20]—where the sound wave reflection and interaction pose additional challenges. Some useful attempts include the extension of the concept of radiation modes to a vibro-acoustic

[a)]Also at: Department of Mechanical Engineering, The Hong Kong Polytechnic University, Hong Kong 999077, China
[b)]Electronic mail: dujingtao@hrbeu.edu.cn

coupling system comprising a flexible structure and a completely enclosed cavity.[21] Subsequent research efforts have been devoted to the use of such interior radiation modes for developing various structural error sensing systems to attenuate the total acoustic potential energy in acoustical cavities.[22–26]

Another type of problem, different from the free space and the completely enclosed configurations, is the sound radiation into a duct by its flexible wall. The configuration is relevant to a wide spectrum of problems encountered in ducts, such as air conditioning and ventilation systems, which have been attracting persistent attention in the noise control community. The problem of the vibro-acoustic interaction of flush-mounted flexible structures and the sound propagation inside the duct has long been taken as a benchmark problem in the open literature, with potential applications such as break in/out noise problems in ducts, transmission loss analyses, and flow-through plate silencer designs.[27–34] To the best of our knowledge, radiation modes in a duct environment have not been investigated. As a result, how radiation modes in a duct behave as compared with their well-known free-field counterparts still remains unclear. Therefore, it is believed that such an analysis would shed light on the vibro-acoustic interaction mechanisms to help conceive efficient duct active/passive noise control devices.

Motivated by this, the sound radiation characteristics of a flexible structure flush-mounted in a duct and the interior sound radiation modes inside the duct are investigated in this paper through the establishment of a coupled vibro-acoustic model in conjunction with Rayleigh-Ritz procedure. In the model, the radiated sound pressure from the wall oscillation is calculated via the surface velocity integral,[29] subsequently giving the radiated sound power. Radiation modes in the duct, in both 2D and 3D configurations, are obtained through eigen-decompositions of the radiation resistance matrix. The objective of this paper is twofold: the study of structural radiation characteristics of a practical vibrating structure used as a duct noise mitigation measure, and the exploration of radiation modes inside an acoustic duct in both 2D and 3D configurations. Finally, some concluding remarks are summarized.

II. THEORETICAL FORMULATION

A. Vibro-acoustic modeling of a structure-duct system

A 2D beam-duct model comprising a flexible beam coupled to a straight duct is considered first and will later be extended to a 3D panel-duct configuration. As illustrated in Fig. 1, the flexible beam, flush-mounted along the inner wall of the duct, is excited by a harmonic force $F(x_s)$, radiating sound into the duct with anechoic terminations. The length of the flexible beam L and the duct height h are also shown in the figure, along with the coordinate system used for the modelling, in which the origin O is located at the left end of the flexible beam.

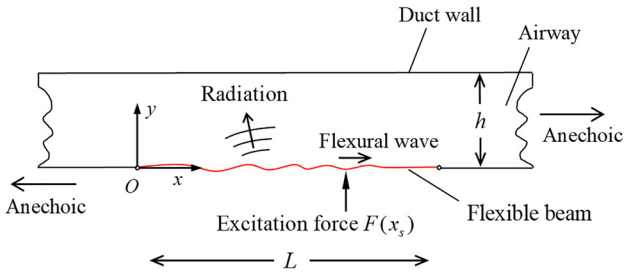

FIG. 1. (Color online) Schematic of the coupled beam-duct vibro-acoustic system.

The transverse displacement of the flexible beam can be expressed through modal expansion as

$$u(x) = \sum_{m_x=1}^{\infty} a_{m_x}\phi_{m_x}(x), \tag{1}$$

where a_{m_x} represents the complex modal amplitude and $\phi_{m_x}(x)$ the mode shape function of the beam.

The sound pressure radiated from the beam into the duct can be estimated through surface velocity integral,[29] written as

$$P_{rad}(x,y) = \frac{\rho_0}{2h}\sum_{m=0}^{\infty}\frac{\omega}{k_m}\psi_m(y)\int_0^L \psi_m(y_s)\Big|_{y_s=0} v \times G(x,x')\mathrm{d}x', \tag{2}$$

where ρ_0 is the air density; y_s the y axis coordinate on the beam; $\psi_m(y)$ the duct acoustic mode shape function; $v = i\omega u$; and $G(x, x')$ and k_m are Green's function and modal wavenumber, respectively, defined as

$$G = H(x-x')\mathrm{e}^{-\mathrm{i}k_m(x-x')} + H(x'-x)\mathrm{e}^{+\mathrm{i}k_m(x-x')}, \tag{3a}$$

$$k_m = \frac{\omega}{ic_0}\sqrt{(m\pi/k_0h)^2 - 1}; \tag{3b}$$

here, H is the Heaviside function, and c_0 the sound speed in air. Zero-order plane waves correspond to $m = 0$, while higher-order modes correspond to $m > 1$.

An energy formulation is adopted, which allows a more flexible inclusion of any vibration or acoustic devices in a unified manner through their energy description. For the transverse vibration of the flexible beam, the corresponding Lagrangian system is expressed as

$$L_{beam} = U_{beam} - T_{beam} + W_P + W_F, \tag{4}$$

where U_{beam} and T_{beam} are the total potential and kinetic energies associated with the vibration of the beam, respectively; W_P means the work done by the sound pressure over the upper surface of the beam; W_F represents the work done by the excitation force, namely,

$$U_{beam} = \frac{1}{2}EI\int_0^L\left[\frac{\partial^2 w(x)}{\partial x^2}\right]^2 dx, \tag{5a}$$

https://doi.org/10.1121/10.0001258

$$T_{beam} = \frac{1}{2}\omega^2 \rho s \int_0^L u^2(x)dx, \tag{5b}$$

and

$$W_p = \int_0^L P_{rad} u \mathrm{d}x, \tag{6a}$$

$$W_F = \int_0^L F u \delta(x - x_s)dx, \tag{6b}$$

in which ρ, EI, and s are the mass density, bending stiffness, and the cross-sectional area of the beam, respectively. Substituting Eqs. (1) and (2) into Eq. (4) and extremizing the Lagrangian system with respect to the modal amplitude coefficients a_{m_x} yield a set of linear equations. For numerical implementation, the decomposition series is truncated into finite terms to form the following system equations in a matrix form:

$$(\mathbf{K} - \omega^2\mathbf{M} + i\omega\mathbf{K_p})\mathbf{a} = -\mathbf{F}, \tag{7}$$

in which $\mathbf{K}$ and $\mathbf{M}$ are the stiffness and mass matrices of the *in vacuo* flexible beam, respectively; $\mathbf{K_p}$ is the coupling matrix characterizing the beam-duct interaction; $\mathbf{a}$ is a vector containing all the unknown coefficients $a_1,\ldots,a_{m_x}$; and $\mathbf{F}$ is the load vector due to the external excitation applied on the flexible beam. The solution of Eq. (7) gives the modal amplitude vector $\mathbf{a}$, thus allowing the calculation of all other vibro-acoustic response metrics. It is noted that the Lagrangian system is used for the description of the structural dynamics, through which the vibro-acoustic coupling is considered via the work done by the sound pressure over the interface.

B. Modal radiation efficiency of the beam and radiation modes in the duct

The total radiated sound power generated by the vibrating beam in the duct can be calculated by[35]

$$W_{rad} = \frac{1}{2}\int_0^L \mathrm{Re}[v^*(x,y)P_{rad}(x,y)]dx, \tag{8}$$

where $P_{rad}(x, y)$ is the sound pressure over the beam surface; $v(x, y)$ is its normal velocity and Re [] and * denote the real part and the complex conjugate of a complex variable, respectively. Substituting Eqs. (1) and (2) into the above equation yields

$$\begin{aligned} W_{rad} = \mathrm{Re}\frac{(i\omega)^2\rho_0}{4h}\sum_{m=0}^{\infty}\frac{\omega}{k_m}\psi_m(y_s)^2 \\ \times \int_0^L\int_0^L \sum_{m_x=1}^{\infty} a_{m_x}\phi(x') \times G(x,x')\mathrm{d}x' \\ \times \sum_{m'_x=1}^{\infty} a_{m'_x}\phi(x)dx = \mathbf{a}^{\mathbf{H}}\mathbf{Q}\mathbf{a}, \end{aligned} \tag{9}$$

in which the superscript $^{\mathrm{H}}$ denotes the Hermitian transpose operation; $\mathbf{Q}$ is a real and symmetric matrix in which the diagonal and the off-diagonal terms represent the self-interaction and mutual-interaction, respectively, expressed as

$$\begin{aligned} Q_{m_x m'_x} = \frac{(i\omega)^2\rho_0}{4h}\mathrm{Re}\left\{\sum_{m=0}^{\infty}\sum_{n=0}^{\infty}\frac{\omega}{k_m}\psi_m(y_s)^2 \right. \\ \left. \times \int_0^L \phi_{m_x}(x)\int_0^L \phi_{m_{x'}}(x') \times G_m(x,x')dx'dx\right\}. \end{aligned} \tag{10}$$

In the subsequent equations, the notation Re{ } is omitted for simplicity. Considering a beam with simply supported boundaries, $\phi_{m_x}(x) = \sin(m_x\pi x/L)$, $\mathbf{Q}$ can then be expressed as

$$\begin{aligned} Q_{m_x m'_x} = \frac{(i\omega)^2 L^2\rho_0}{4h}\sum_{m=0}^{\infty}\frac{\omega}{k_m}\psi_m(y_s)^2 \\ \times \left(\frac{m'_x\pi m_x\pi(\cos m_x\pi - e^{-ik_mL})(\cos m_x\pi + \cos m'_x\pi)}{(m'^2_x\pi^2 - k_m^2L^2)(m_x^2\pi^2 - k_m^2L^2)} \right. \\ \left. + \frac{ik_m\delta_{m_x m'_x}}{(m_x^2\pi^2 - k_m^2L^2)}\right), \end{aligned} \tag{11}$$

where δ is the Kronecker delta function.

The radiation efficiency of the vibrating beam is defined as[35]

$$\sigma = W_{rad}/\rho_0 c_0 S^T\langle\bar{u}^2(t)\rangle, \tag{12}$$

where S^T is the total area of the radiator and $\langle\bar{u}^2\rangle$ is the mean-square velocity averaged over both time and space, namely,

$$\langle\bar{\dot{u}}^2(t)\rangle = \frac{1}{S^T}\int_0^{S^T}\dot{u}(s)\bar{\dot{u}}(s)ds = (i\omega)^2\frac{1}{S^T}\sum_{n=1}^{\infty}\frac{S^T}{2}a_n^2. \tag{13}$$

For a single structural mode, the radiated acoustic power can be expressed as a special case of Eq. (9), namely $W_{rad} = |a_i|^2 Q_{mxmx'}$. The modal radiation efficiency of structure modes is defined as

$$\sigma_{if} = 1/(i\omega)^2 \times Q_{if}/\left(\rho_0 c_0 S^T/2\right), \tag{14}$$

in which Q_{ij} is the (i, j) term in matrix $\mathbf{Q}$, which is associated with the ith and jth structural mode shape ϕ_i(x) and $\phi_j(x)$. For $i = j$, σ_{ii} can be seen as the self-radiation efficiency of the ith structural mode, and $i \neq j$ represents the normalized mutual-interaction terms with respect to the off-diagonal elements. Upon dividing the structure surface into pieces with sufficiently small size compared to the wavelength, the vector of complex linear velocities of each of these elemental sources is denoted $\dot{\mathbf{u}}$. The vector of complex acoustic pressure in front of each source can be determined through the acoustic impedance $\mathbf{Z}$, expressed as

$$\mathbf{p} = \mathbf{Z}\dot{\mathbf{u}}. \tag{15}$$

Then the sound power radiated by an array of elements can be estimated by[4]

$$W = \frac{S}{2}\mathrm{Re}(\mathbf{v}^H\mathbf{p}) = \frac{S}{2}\mathrm{Re}(\mathbf{v}^H\mathbf{Z}\mathbf{v}) = \mathbf{v}^H\mathbf{R}\mathbf{v} = \mathbf{v}^H\mathbf{Y}^H\mathbf{\Lambda}\mathbf{Y}\mathbf{v}, \tag{16}$$

where the radiation resistance matrix for elemental radiators, $\mathbf{R}$, is real and symmetric, so that it allows for an eigenvalue/eigenvector decomposition in the form of $\mathbf{R} = \mathbf{Y}^H\mathbf{\Lambda}\mathbf{Y}$. In this way, the radiation mode shapes can be obtained directly from the columns of matrix $\mathbf{Y}$, which correspond to the eigenvectors of the radiation matrix $\mathbf{R}$.

Assuming that the beam vibration is described by a set of N structural modes of known mode shape, with complex amplitudes given by the elements of the vector $\mathbf{a}$, the velocity vector at I points on the structure, $\mathbf{v}$, can then be written as

$$\mathbf{v} = \mathbf{\Phi}\mathbf{a}, \tag{17}$$

where the elements of the $I \times N$ matrix $\mathbf{\Phi}$ depend only on the known mode shapes.

Combining the Eqs. (9) and (17), one gets[4]

$$W = \mathbf{v}^{\mathbf{H}}\mathbf{R}\mathbf{v} = \mathbf{a}^{\mathbf{H}}\mathbf{\Phi}^{\mathbf{T}}\mathbf{R}\mathbf{\Phi}\mathbf{a} = \mathbf{a}^{\mathbf{H}}\mathbf{Q}\mathbf{a}. \tag{18}$$

In this formulation, the radiation resistance matrix $\mathbf{R}$ can be obtained once the modal shape matrix $\mathbf{\Phi}$ and the integral matrix $\mathbf{Q}$ in Eq. (9) are determined. The advantage of expressing the radiated power in the form of $W = \mathbf{v}^{\mathbf{H}}\mathbf{Y}^{\mathbf{T}}\mathbf{\Lambda}\mathbf{Y}\mathbf{v}$ is that the radiation mode amplitudes are expressed directly in terms of the motion of an array of elements over the surface of the radiating body, instead of structural modal amplitudes.

C. Extension to 3-D rectangular panel-duct interaction model

The above modeling framework can be extended to 3D configuration by replacing the beam by a rectangular plate. Similarly, the flexural displacement function of the panel can be rewritten as

$$u(x,y) = \sum_{m_x=1}^{\infty}\sum_{m_y=1}^{\infty} a_{m_x m_y}\varphi_{m_x m_y}(x,y), \tag{19}$$

where L_x and L_y are the panel length and width, respectively, and $\varphi_{m_x m_y}$ is the mode shape function.

The corresponding Lagrangian system for the panel is expressed as

$$L_{panel} = U_{panel} - T_{panel} + W_P + W_F, \tag{20}$$

where U_{panel} and T_{panel} are the total potential and kinetic energies of the vibrating panel, respectively, namely,

$$U_{panel} = \frac{B}{2}\int_0^{L_x}\int_0^{L_y}\left\{\left(\frac{\partial^2 u}{\partial x^2}\right)^2 + \left(\frac{\partial^2 u}{\partial y^2}\right)^2 + 2\mu\frac{\partial^2 u}{\partial x^2}\frac{\partial^2 u}{\partial y^2} + 2(1-\mu)\left(\frac{\partial^2 u}{\partial x \partial y}\right)^2\right\}dxdy, \tag{21}$$

$$T_{panel} = \frac{1}{2}\int_0^{L_x}\int_0^{L_y}\rho_s\sigma\left(\frac{\partial u}{\partial t}\right)^2 dxdy = \frac{1}{2}\rho_s\sigma\omega^2\int_0^{L_x}\int_0^{L_y}u^2 dxdy, \tag{22}$$

in which ρ_s and σ are the mass density and the thickness of the panel, respectively. $B = E_p h^3/12(1-\mu^2)$ is the bending stiffness with μ being the Poisson's ratio and E_p the Young's modulus.

The radiated sound pressure can be expressed as

$$p_{rad}(x,y,z) = \frac{\rho_0}{2L_y h}\sum_{m=0}^{\infty}\sum_{n=0}^{\infty}\frac{\omega}{k_{mn}}\psi_{mn}(y,z) \times \int_0^{L_x}\int_0^{L_y}\psi_{mn}(y',z')v(x',y',t) \times G_{mn}(x,x')dy'dx' \tag{23}$$

where $\psi_{mn}(y,z)$ is the duct acoustic modal function; $v = i\omega u$; and $G(x,x')$, and k_{mn} are modal Green's function and wavenumber, respectively, expressed as

$$G_{mn}(x,x') = \left[H(x-x')e^{-ik_{mn}(x-x')} + H(x'-x)e^{+ik_{mn}(x-x')}\right] \tag{24}$$

and

$$k_{mn} = \frac{\omega}{ic_0}\sqrt{(n\pi/k_0 h)^2 + (m\pi/k_0 L_y)^2 - 1}. \tag{25}$$

Using Eq. (8), the radiated sound power can be determined. For the 3D model, the elements in matrix $\mathbf{Q}$ can be expressed as

$$Q_{m_x m_x' m_y m_y'} = \mathrm{Re}\sum_{m=0}^{\infty}\sum_{n=0}^{\infty}T\int_0^{L_y}\int_0^{L_x}\psi_{mn}(y,0)\varphi_{m_x m_y} \times (x,y)\int_0^{L_y}\int_0^{L_x}\psi_{mn}(y',0)\varphi_{m_x' m_y'}(x',y') \times G_{mn}(x,x')dx'dy'dxdy, \tag{26}$$

in which

$$T = \frac{(i\omega)^2\rho_0}{4L_y h}\frac{\omega}{k_{mn}}. \tag{27}$$

III. NUMERICAL RESULTS AND DISCUSSIONS

Although the main focus of this paper is put on the radiation modes, the study of sound radiation from a vibrating

https://doi.org/10.1121/10.0001258

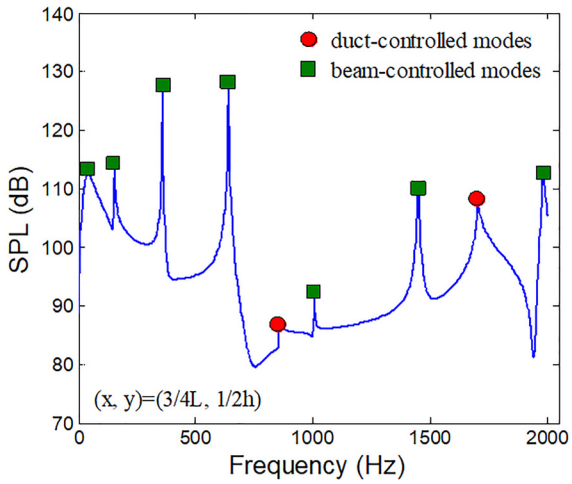

FIG. 2. (Color online) Sound pressure response at certain points inside the duct.

wall in a duct is also of great importance from the viewpoint of duct noise control. Therefore, the structural properties should be taken into account, accordingly. Before we explore discussions on numerical results, it is essential to clarify some technical terminologies relating to "modes" and "radiation efficiency" that will be used in the subsequent analyses. A structural mode refers to a mode of the flexible structure *in vacuo*, whilst a duct mode refers to an acoustic mode of the duct with rigid walls. For the structural-acoustic model studied in this work, the modal frequencies of the coupled system are extracted from the resonant peaks of sound pressure response curves. A radiation mode (RM) represents the characteristic velocity distribution, which independently contributes to the sound radiation. It is obtained directly from the eigenvectors of the radiation resistance matrix **R**. The modal radiation efficiency (MRE) studied in Sec. III A refers to that of a structural mode rather than a radiation mode.

A. Structural mode radiation characterization

The established 2D model duct-beam is first studied with consideration of the coupling characteristics and modal radiation efficiency of the vibrating beam. In this work, simply supported boundary conditions are considered for the beam and subsequent panel structures. The beam and the duct bear the following parameters, namely air density $\rho_0 = 1.255\,\mathrm{kg/m^3}$, sound speed in air $c_0 = 340\,\mathrm{m/s}$, duct height $h = 0.2$ m, beam length $L = 2h$, the unit mass density $\rho_s = 4\,h\rho_0$, and bending stiffness $EI = 0.015\ \rho_0 c_0^2 h^3$. A point force excitation is applied to the beam at $x = 3/5L$. To avoid the infinite response at system resonances, damping is introduced in the simulations via a complex Young's modulus for the beam and via a complex sound speed for the duct, respectively, with a nominal loss factor of 0.03. The correctness and the accuracy of current models have been verified through comparisons with the finite element results (not shown here), in which the same damping loss factor was used.

Figure 2 presents the calculated sound pressure response at $(3/4\,L,1/2h)$ inside the duct. The system under investigation involves structural-acoustic coupling between the vibrating beam and the acoustic duct. As such, the coupled modal frequencies are extracted from the resonant peaks of the sound pressure response curve, which are found to be very close to either the structural modes of the beam *in vacuo* or the acoustic modes of the duct with rigid walls. Therefore, these modes are categorized into the so-called beam-controlled modes (B-mode) and duct-controlled modes (D-mode), which are labelled and marked accordingly in this figure. The corresponding peak frequencies are tabulated in Table I. Coupling in the duct-beam system can be clearly observed from the shift of the coupled resonance peaks as compared with those natural frequencies before coupling.

Plotted in Fig. 3(a) is the variation of the MREs of the first three beam modes σ_{11}, σ_{22}, and σ_{33} with respect to frequency. The normalized mutual-interaction term σ_{13} is also plotted, showing a drastically reducing level as the frequency increases. Since there exists no interaction between the radiation of the odd and even modes of the beam, the corresponding mutual interaction terms (e.g., σ_{12}) are zero. Obviously, when the frequency increases and exceeds the first cut-on frequency of the duct, $c_0/2h$, obvious oscillation can be observed, with peaks actually coinciding with the duct-controlled modes.

To further quantify the contributions of the higher-order duct modes to this oscillating behavior, the modal radiation efficiencies of the first two beam modes are calculated by only including the plane wave effect and ignoring the higher-order waves radiated from the vibrating structure, namely $m_{duct} = 0$, with the corresponding results presented in Fig. 3(b). It can be seen that the oscillating phenomenon is caused by the higher-order waves. Moreover, the above two figures show that the MREs for the symmetric modes are dominant and nearly constant in the low frequency range before the cut-on. This can also be deduced from Eqs. (10) and (11). In fact, when $m_x + m_x'$ is an odd number, Q is zero, leading to zero $\sigma_{\text{odd-even}}$, as mentioned above. Taking $m = 0$ (plane wave), $m_x' = m_x = 1$, $L = 0.4$ m, the equation in the bracket of Eq. (10) can be simplified as

TABLE I. Comparison of the coupled and uncoupled resonant frequencies (Hz). Duct-controlled mode (D-mode) and beam-controlled mode (B-mode).

			B-mode		D-mode	B-mode		D-mode	B-mode
Uncoupled	40.1	163.7	368.1	654.2	850	1022.1	1471.6	1700	2002.9
Coupled	41	154.2	358.4	640.6	850.9	1005	1449	1702	1984

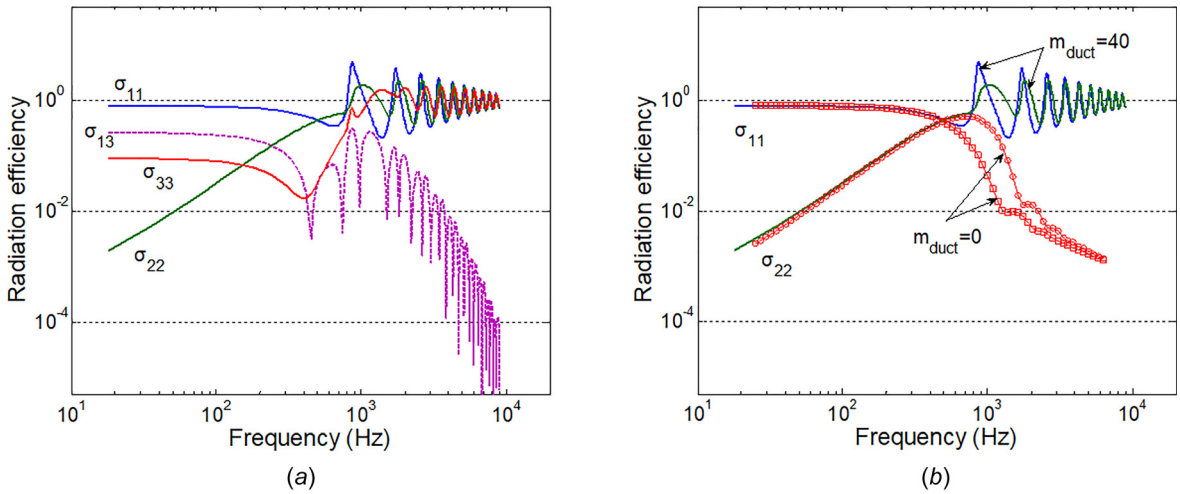

FIG. 3. (Color online) Modal radiation characteristic analysis: (a) MRE for the first three beam modes (solid lines) and the normalized mutual-interaction term σ_{13} (dashed line); (b) MRE of mode 1 and 2 calculated using the duct mode numbers $m_{duct}=0$ (plane wave only) and 40 (including higher-order duct modes), respectively.

$$\mathrm{Re}\left[\int_0^L \sin\left(\frac{1\pi}{L}x\right)\int_0^L \sin\left(\frac{1\pi}{L}x'\right)\times G(x,x')dx'dx\right] = \frac{2\pi^2L^2(1+\cos k_0L)}{(\pi^2-k_0^2L^2)(\pi^2-k_0^2L^2)}, \quad (28)$$

which suggests that it is approximately equal to a constant 0.064 as k_0L holds a relatively small value ($k_0L<0.5$).

The influence of the duct height on structural modal radiation efficiency is also shown in Fig. 4. It can be seen that, with the increase of the duct height, oscillations begin at a lower frequency but with flattened magnitudes.

B. 1D radiation modes in the duct

The 1D radiation modes (RM) (corresponding to a flexible beam) are analyzed hereafter. The RMs are sorted according to the eigenvalue order of the radiation resistance matrix **R**, following a decreasing importance order in terms of sound radiation. The first five eigenvectors of **R**, which correspond to the 1 D shapes of the first five radiation modes in the duct, are plotted in Fig. 5 and compared with their counterparts in free space at three different frequencies: $kL=0.5$, 3, and 5, respectively. Note the three frequencies are tactically chosen to be below, around, and above the cut-frequency of the duct with $L=h=0.1$ m in the present case. In the figure, the solid and dashed lines correspond to the RMs in free space and within the duct, respectively. It can be seen that, at low frequencies, typically before the duct cut-on (first row in Fig. 5), the duct seems to have negligible effects on the RMs. In particular, the first two radiation patterns feature a piston-like and a rocking pattern in both free-space and duct cases, in agreement with those calculated by Elliott.[4] With the increase of frequency, the effects of the duct start to appear, more obviously on the lower-order RMs, exemplified by the first three RMs. Nevertheless, higher-order RMs, like the fourth and fifth ones, though exhibiting more complex spatial variations, still hold similar shapes in both the duct and free-space cases.

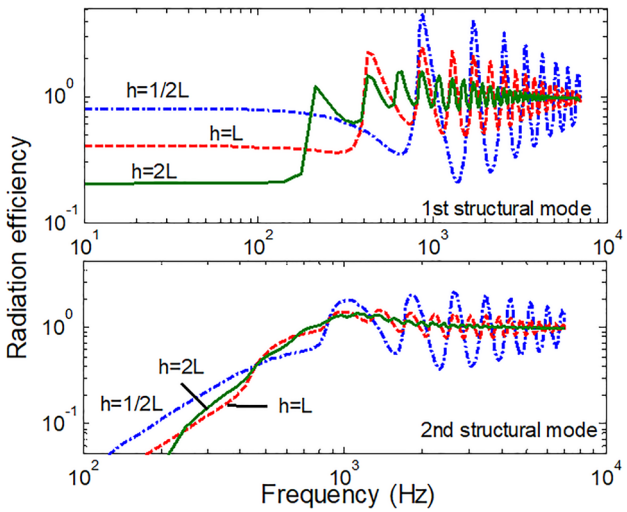

FIG. 4. (Color online) Modal radiation efficiency of the first and second structural modes with different duct heights.

In order to better illustrate the spatial variation of the lower-order RMs with respect to frequency, the waveforms of the first RM, in both free space and the duct, are plotted in Figs. 6(a) and 6(b), respectively. It can be seen that, as kL increases, the RM shapes gradually evolve from a piston-like to a quadratic variation in free space. A very similar trend can be observed for the RMs in the duct until kL reaches a certain value, after which a drastic change takes place, to such an extent that even the symmetry of the RM shape is altered.

To better describe and understand the phenomenon, a new parameter, v_{dn}, is defined to quantify the spatial variation of RM shapes. For a given RM, of order n, the corresponding mode shape is compared with its counterpart ($\mathrm{RM}_{\mathrm{nref}}$) at $kL=0.1$ as a measure to quantify its spatial variation degree as

https://doi.org/10.1121/10.0001258

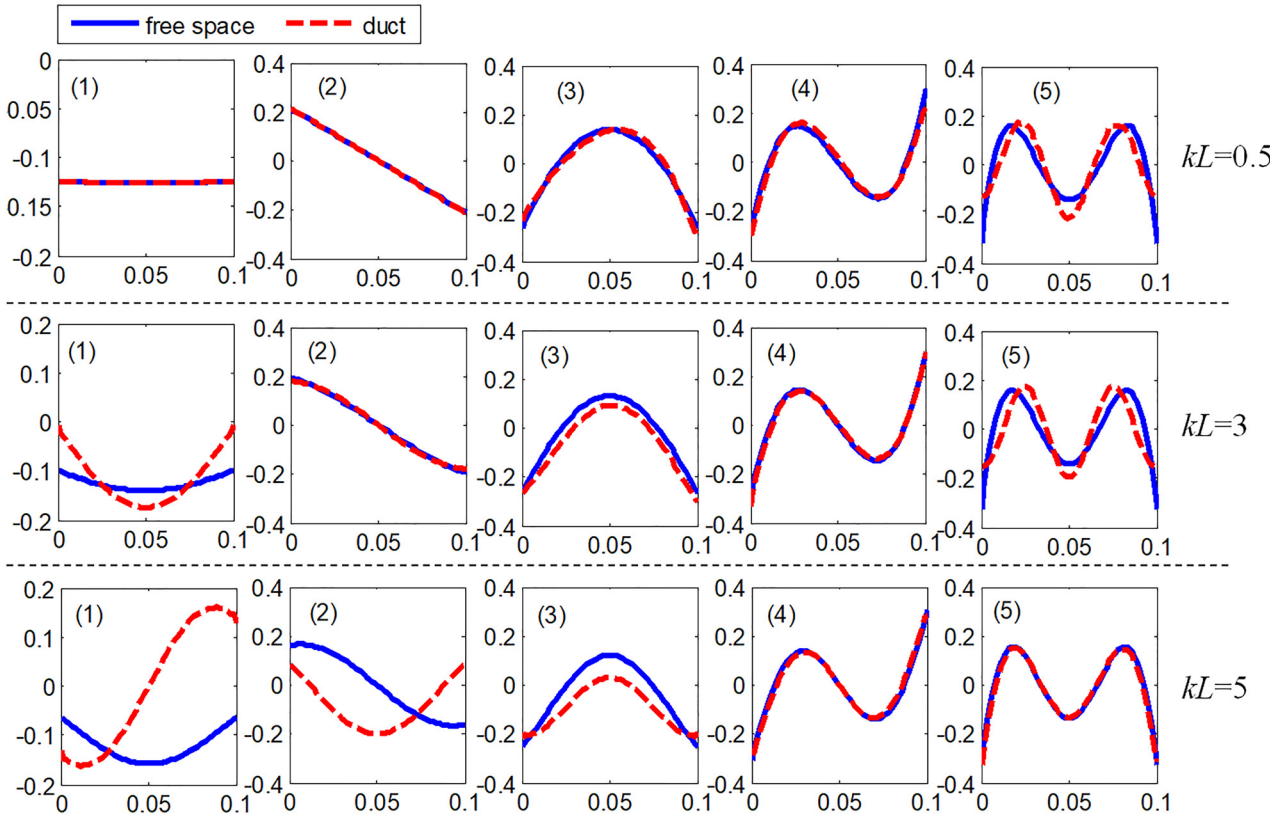

FIG. 5. (Color online) The first five radiation mode shapes of a flexible beam in duct (solid lines) and in free field (dashed line) at three frequencies. Upper row: $kL = 0.5$; medium row: $kL = 3$; bottom row: $kL = 5$. Note, $L = h$ in this simulation case.

$$v_{dn} = \|\mathrm{RM_n} - \mathrm{RM_{nref}}\|_2 = \sqrt{\sum_i^I |\mathrm{RM_n}(x_i) - \mathrm{RM_{nref}}(x_i)|^2}, \quad (29)$$

in which $\mathrm{RM_n}$ is the nth radiation mode shape with respect to different frequencies/wavenumbers, and I is the number of elements along the beam length, taken as 23 in the present case. For the first RM, v_{d1} in the duct (solid curve with circles) and in the free space (dashed line) are both plotted in Fig. 7(a). It can be seen that, at low frequencies, v_{d1} in both cases exhibits an increasing trend with the frequency, consistent with the observations obtained from Figs. 6(a) and 6(b). For the duct RM, however, a sudden drop occurs around some particular kL values, producing a valley with a drastically reduced v_{d1}. A close examination shows that the observed valleys actually start from some particular wavenumbers (i.e., $kL = \pi$, 2π, and 3π), which actually correspond to the cut-on frequency of the duct and its multiples/

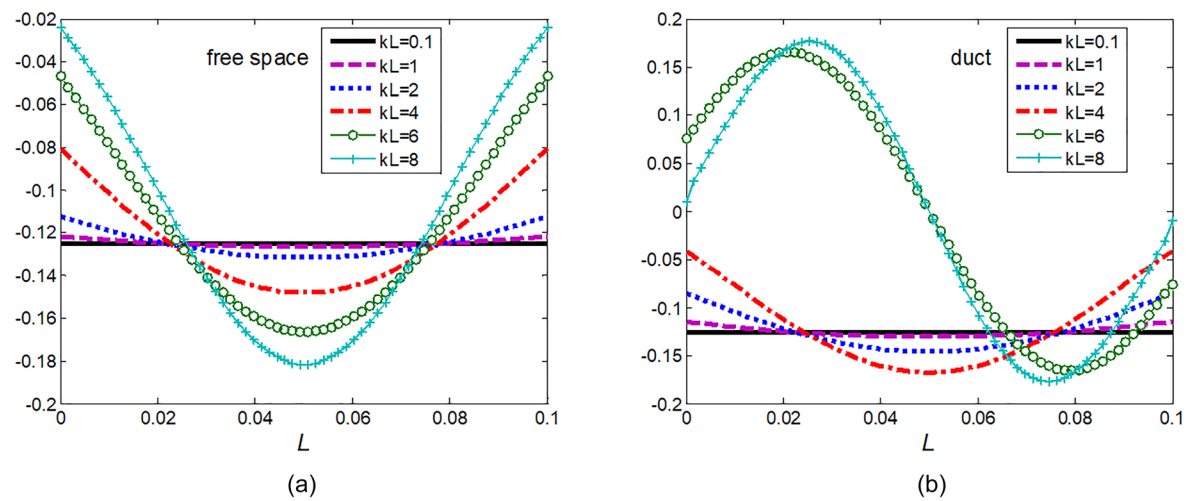

FIG. 6. (Color online) Spatial variation of the first radiation mode shape with kL. (a) in free space and (b) in duct.

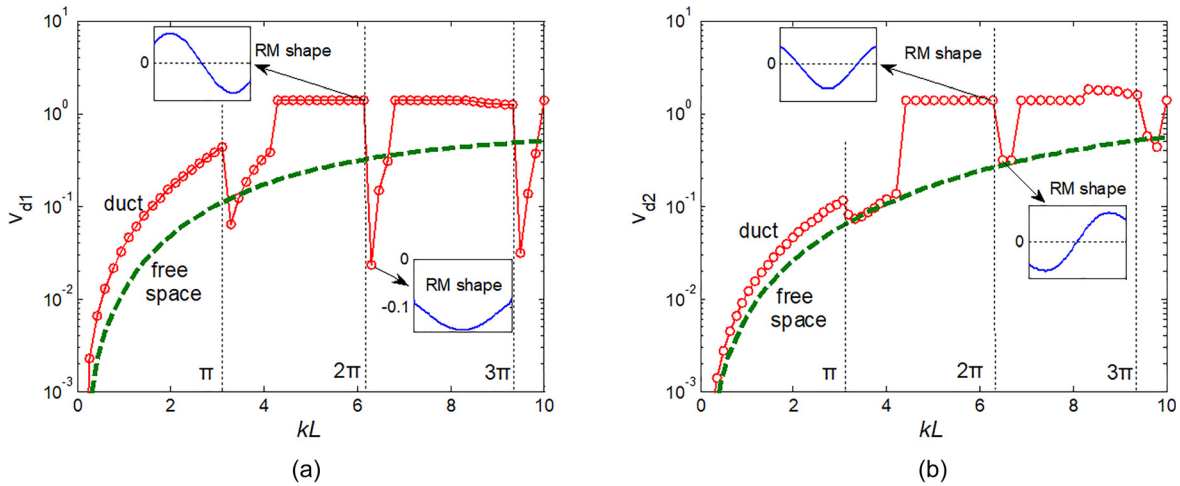

FIG. 7. (Color online) Quantification of the spatial variation degree for the first and second radiation modes for different wavenumbers. (a) v_{d1} and (b) v_{d2}. Note, $L = h$ in the present case.

harmonics. Compared with their free-space counterparts, radiation modes in the duct involve the participation of acoustic modes in sound radiated power estimation, particularly when the excitation frequency exceeds the cut-on frequency where higher-order acoustic modes appear. Moreover, the sub-plots in Fig. 7(a), taken at $kL = 6.14$ and 6.3, show that before and after these critical kL values ($kL = 2\pi$ in the present case), a drastic change in the RM shape occurs, whilst the RM shape remains more or less the same between these critical kL values. It can be further seen that the radiation abilities of different RM shapes are altered around the duct cut-on frequency. To examine the generality of the above statement, similar analysis is performed for the second RM using v_{d2}, with results depicted in Fig. 7(b) showing similar phenomena. The jumping phenomena are attributed to the effect of higher-order radiated sound waves, in terms of either plane waves or higher-order waves. More specifically, higher-order waves have no contribution to sound radiation when kL is small than the cut-on frequency of the duct, but start to manifest after the cut-on, thus causing the jumps observed in v_{d1}. Obviously, when the duct height increases, the corresponding cut-on frequency reduces, thus causing the jumping phenomena in v_{d1} at a lower frequency. Note the radiation efficiencies of the radiation modes are proportional to the eigenvalues of matrix $\mathbf{R}$, and there are no mutually dependent terms. The influencing trend of the duct height on them are similar to Fig. 4.

Therefore, it can be concluded that, when frequency increases, the duct exerts a more significant impact on the lower-order radiation modes, which can be drastically different from their free-space counterparts. The impact starts to appear when reaching the cut-on frequency of the duct. At this frequency and each of its multiples/harmonics, a drastic RM sharp change is observed.

C. 2D radiation modes in the duct

The above analysis is extended to a duct-plate system to investigate the 2D radiation modes (corresponding to a plate) mounted in the duct with its height $h = L_x$. In the following numerical examples, the plate aspect ratio is taken as $L_x/L_y = 1/0.57$, for a radiator with 28 and 16 segments along its length and width, respectively, as used by Elliott and Johnson.[4]

Figure 8 presents the 2D RM shapes in free space and within the duct, respectively, at $kL_x = 0.1$, below the cut-on frequency of the duct. Obviously, the first three RMs in both cases show very similar patterns. The first radiation mode follows an in-phase monopole-like distribution, followed by two dipole-like rocking modes. Two Quadrupole-like modes 4 (longitudinal) and 5 (lateral) in the duct resemble the modes 5 and 4 in the free space. This matching in a reversed order is most likely due to the differences in the relative importance of their radiation efficiency in the two cases. Nevertheless, the ensemble of the first five RMs as a whole is very similar in both cases. The first four radiation modes of the plate in duct and in free space for a higher frequency $kL_x = 5$, which is above the cut-on frequency of the duct, are shown in Fig. 9. Obvious differences in the mode shapes can be observed. In addition, RMs in the duct seem to exhibit dominant spatial variation mainly in the stream-wise direction (length direction) of the duct. Due to the increasing complexity in the distribution patterns as the wavenumber increases, a parameter, referred to as a "shape change rate factor σ_r," is defined and used to quantify the spatial variation of the radiation modes, expressed for each radiation mode in each direction as

$$\sigma_r = |\max(Rm_r) - \min(Rm_r)|/|\max(Rm_r)|, \quad r = x, y, \tag{30}$$

in which Rm_r denotes the value of a radiation mode in r-direction (either x or y). Using the above defined σ_r, RMs can be loosely classified as follows: If $\sigma_r < 10\%$, then the radiation mode is regarded as basically having no variation in the corresponding r-direction. Using this classification criterion, the first four radiation modes of the plate in free

https://doi.org/10.1121/10.0001258

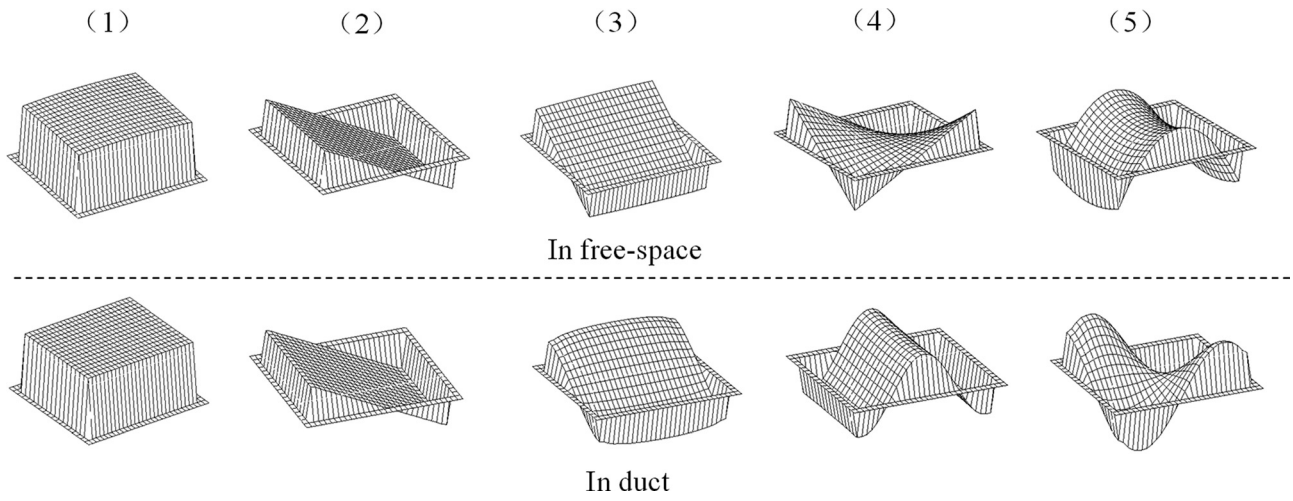

FIG. 8. The first five 2D radiation modes in free space (upper) and in duct (bottom), respectively, at $kL_x = 0.1$.

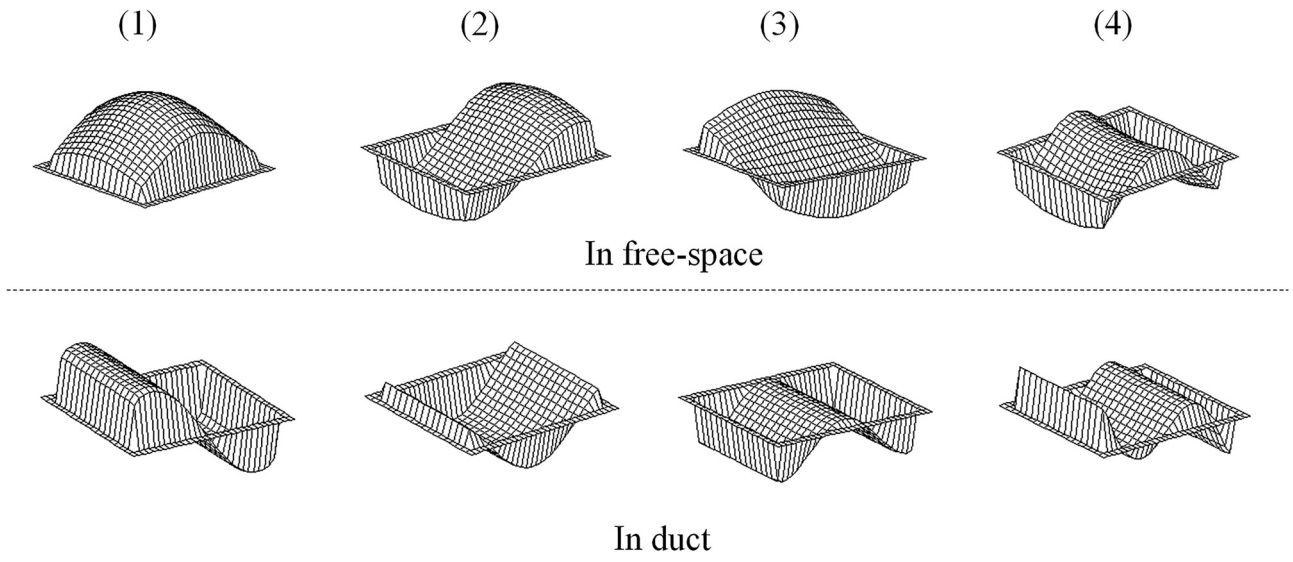

FIG. 9. The first four 2D radiation modes in free space (upper) and in duct (bottom), respectively, at $kL_x = 5$.

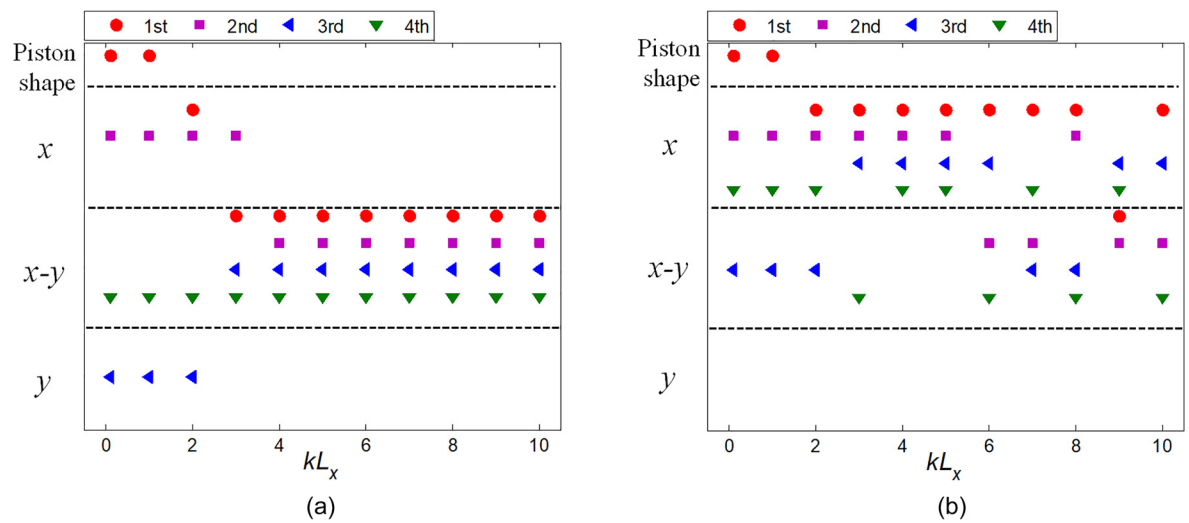

FIG. 10. (Color online) Distribution patterns of radiation modes in (a) free space and (b) duct.

space and in the duct are regrouped into different categories in Fig. 10. Radiation modes are labeled by x and y according to the dominance level of their spatial deformation. Therefore, the x or y category designates RMs, which are mainly 1 D patterns, whilst the x-y category represents 2D patterns. Note the piston-like radiation modes are separated and also shown on the top row of the two figures. It is clear that the RMs in free space exhibit dominant 2D behavior as the frequency increases (those RMs labeled by x-y). In the duct, however, these low-order RMs involve more dominant deformation along duct length direction. Those pure 1 D span-wise direction (y-direction) RMs in free space (the third RM at low frequency) are completely suppressed due to the presence of the duct. In particular, in the bandwidth $kL_x = 3.14$–5.5 for the present case, all four RMs behave like 1 D patterns along the x axis. In this case, the 3D plate-duct system can be simplified as a 2D system.

IV. CONCLUSIONS

The sound radiation of a vibrating structure (beam/plate) mounted in a semi-enclosed space (duct) is analyzed in this paper. The problem is formulated via an energy-based formulation in conjunction with the near-field integration technique. The model allows the calculation of the radiation resistance matrix in the duct, from which the interior radiation modes of the structure are computed via eigenvalue decompositions. Major conclusions are summarized as follows.

(1) Above the cut-on frequency of the duct, the modal radiation efficiency of the beam in the duct exhibits obvious oscillations with respect to frequency, modulated by the higher-order duct modes. Different from the free-space case, duct modes are involved in the structural radiation of the beam, especially for large wavenumbers. Compared with the antisymmetric modes of the beam, symmetric modes dominate the radiation process with a gentle variation in their radiation efficiencies at small acoustic wavenumbers.
(2) Numerical investigations on the radiation modes show that the radiation modes in a duct basically behave like in free space below the cut-on frequency of the duct. Above it, the lower-order radiation modes are more sensitive and prone to be affected by the duct modes. Significant changes in the radiation mode shapes are observed before and after the cut-on frequency and each of its multiples/harmonics.
(3) Extension of the analysis to 3D plate-duct configuration shows that the duct impairs the radiation modes with a shape variation in the span-wide direction. As such, contrary to the free-space case, lower-order radiation modes in the duct exhibit predominant deformation along the streamwise direction. This alludes to the possibility of approximating a 3D system by a 2D configuration within certain frequency ranges.

As a final remark, this work is expected to shed new light onto the sound radiation mechanism of a vibrating structure in a partially closed acoustic duct, which hopefully can provide further guidance on the design of acoustics devices as well as active/passive noise controls in ducts with flexible walls.

ACKNOWLEDGMENT

This work was supported by the National Natural Science Foundation of China (Grant No. 11972125) and Fok Ying Tung Education Foundation (Grant No. 161049).

[1]G. V. Borgiottti, "The power radiated by a vibration body in an acoustic fluid and its determination from boundary measurements," J. Acoust. Soc. Am. **88**, 1884–1893 (1990).
[2]K. A. Cunefare, "The minimum multimodal radiation efficiency of baffled finite beam," J. Acoust. Soc. Am. **90**, 2521–2529 (1991).
[3]K. Naghshineh and G. H. Koopmann, "A design method for achieving weak radiator structures using active vibration control," J. Acoust. Soc. Am. **92**, 856–870 (1992).
[4]S. J. Elliott and M. E. Johnson, "Radiation modes and the active control of sound power," J. Acoust. Soc. Am. **94**(4), 2194–2204 (1993).
[5]K. A. Cunefare and M. N. Currey, "On the exterior acoustic radiation modes of structures," J. Acoust. Soc. Am. **96**(4), 2302–2312 (1994).
[6]C. R. Fuller, S. J. Elliott, and P. A. Nelson, *Active Control of Vibration* (Academic, San Diego, 1996).
[7]M. E. Johnson and S. J. Elliott, "Active control of sound radiation using volume velocity cancellation," J. Acoust. Soc. Am. **98**(4), 2174–2186 (1995).
[8]M. N. Currey and K. A. Cunefare, "The radiation modes of baffled finite plates," J. Acoust. Soc. Am. **98**(3), 1570–1580 (1995).
[9]K. A. Cunefare, M. N. Currey, M. E. Johnson, and S. J. Elliott, "The radiation efficiency grouping of free-space acoustic radiation modes," J. Acoust. Soc. Am. **109**(1), 203–215 (2001).
[10]M. R. Bai and M. Tsao, "Estimation of sound power of baffled planar sources using radiation matrices," J. Acoust. Soc. Am. **112**(3), 876–883 (2002).
[11]H. J. Wu, W. K. Jiang, and Y. J. Liu, "Analyzing acoustic radiation modes of baffled plates with a fast multipole boundary element method," J. Vib. Acoust. **135**, 0110071 (2013).
[12]H. J. Wu, W. K. Jiang, Y. L. Zhang, and W. B. Lu, "A method to compute the radiated sound power based on mapped acoustic radiation modes," J. Acoust. Soc. Am. **135**(2), 679–692 (2014).
[13]S. Marburg, E. Lösche, H. Peters, and N. Kessissoglou, "Surface contributions to radiated sound power," J. Acoust. Soc. Am. **133**, 3700–3705 (2013).
[14]K. Naghshineh and G. H. Koopmann, "Active control of sound power using acoustic basis functions as surface velocity filters," J. Acoust. Soc. Am. **93**(5), 2740–2752 (1993).
[15]G. P. Gibbs, R. L. Clark, D. E. Cox, and J. S. Vipperman, "Radiation modal expansion: Application to active structural acoustic control," J. Acoust. Soc. Am. **107**(1), 332–339 (2000).
[16]A. M. Pasqual, J. R. De França Arruda, and P. Herzog, "Application of acoustic radiation modes in the directivity control by a spherical loud speaker array," Acta. Acust. Acust. **96**, 32–42 (2010).
[17]J. Pan, C. H. Hansen, and D. A. Bies, "Active control of noise transmission through a panel into a cavity: I. Analytical study," J. Acoust. Soc. Am. **87**(5), 2098–2108 (1990).
[18]L. Cheng and J. Nicolas, "Radiation of sound into a cylindrical enclosure from a point-driven end plate with general boundary conditions," J. Acoust. Soc. Am. **91**(3), 1504–1513 (1992).
[19]S. M. Kim and M. J. Brennan, "Active control of harmonic sound transmission into an acoustic enclosure using both structural and acoustic actuators," J. Acoust. Soc. Am. **107**(5), 2523–2534 (2000).
[20]S. K. Lau and S. K. Tang, "Active control on sound transmission into enclosure through a flexible boundary with edges elastically restrained against translation and rotation," J. Sound. Vib. **259**(3), 701–710 (2003).

https://doi.org/10.1121/10.0001258

[21]S. D. Snyder and N. Tanaka, "On feedforward active control of sound and vibration using vibration error signals," J. Acoust. Soc. Am. **94**, 2181–2193 (1993).
[22]B. S. Cazzolato and C. H. Hansen, "Active control of sound transmission using structural error sensing," J. Acoust. Soc. Am. **104**, 2878–2889 (1998).
[23]W. M. Johnson and K. A. Cunefare, "Use of principle velocity patterns in the analysis of structural acoustic optimization," J. Acoust. Soc. Am. **121**(2), 938–948 (2007).
[24]C. Hesse, J. M. V. Perez, and M. Sinapius, "Frequency-independent radiation modes of interior sound radiation: An analytical study," J. Sound. Vib. **392**, 31–40 (2017).
[25]A. K. Bagha and S. V. Modak, "Structural sensing of interior sound for active control of noise in structural-acoustic cavities," J. Acoust. Soc. Am. **138**(1), 11–21 (2015).
[26]C. Hesse, V. Papantoni, S. Algermissen, and H. P. Monner, "Frequency-independent radiation modes of interior sound radiation: Experimental study and global active control," J. Sound. Vib. **401**, 204–213 (2017).
[27]A. Cummings, "The attenuation of sound in unlined ducts with flexible walls," J. Sound Vib. **174**, 433–450 (1994).
[28]A. Cabelli, "The propagation of sound in a square duct with a non-rigid side wall," J. Sound Vib. **103**, 379–394 (1985).
[29]P. E. Doak, "Excitation, transmission and radiation of sound from source distributions in hard-walled ducts of finite length (I): The effects of duct cross-section geometry and source distribution space-time pattern," J. Sound Vib. **31**(1), 1–72 (1973).
[30]L. X. Huang, "Broadband sound reflection by plates covering side-branch cavities in a duct," J. Acoust. Soc. Am. **119**, 2628–2638 (2006).
[31]S. Ramamoorthy, K. Grosh, and T. G. Nawar, "Structural acoustic silencers: Design and experiment," J. Acoust. Soc. Am. **114**(5), 2812–2824 (2003).
[32]Y. Liu and J. T. Du, "Structural-acoustic interaction of a three-dimensional panel-cavity-duct system with non-uniform boundary restraints," J. Fluid. Struct. **79**, 94–114 (2018).
[33]Z. B. Lu, Y. D. Cui, and M. Debiasi, "Active membrane-based silencer and its acoustic characteristics," Appl. Acoust. **111**, 39–48 (2016).
[34]X. Yu, Z. B. Lu, L. Cheng, and F. S. Cui, "Vibroacoustic modeling of an acoustic resonator tuned by dielectric elastomer membrane with voltage control," J. Sound. Vib. **387**, 114–126 (2017).
[35]X. F. Zhang and W. L. Li, "A unified approach for predicting sound radiation from baffled rectangular plates with arbitrary boundary conditions," J. Sound. Vib. **329**, 5307–5320 (2010).